N.-E. Wiberg (Ed.)
© CIMNE, Barcelona 1995

ENHANCED PREDICTION OF STRUCTURAL INSTABILITY POINTS USING A CRITICAL DISPLACEMENT METHOD

E. Oñate and W. T. Matias †
E.T.S. Ingenieros de Caminos, Canales y Puertos
Universidad Politécnica de Cataluña
c/Gran Capitan s/n, 08034 Barcelona
Spain

Dedicated to Prof. Alf Samuelsson

1. INTRODUCTION

The numerical detection and location of bifurcation and limit points, herein denoted generically as *critical points*, has received considerable attention in the computational solid and structural community. Indeed loss of stability and bifurcation are common phenomena in non linear solid and structural mechanics. Typical examples range form classical problems such as the buckling of rods, plates and shell structures, to diffuse necking bifurcation problems, including the formation of localized shear bands, in elastic–plastic solids.

The numerical methods proposed for computation of critical points can be grouped into two categories, namely *indirect* and *direct* methods, respectively. With indirect methods the encounter of the critical point is judged with the help of a detecting parameter while the equilibrium path is being traced in a load incremental manner up to the vicinity of the critical point [1–6]. Typical examples of detecting parameters are the determinant or the smallest eigenvalue of the tangent stiffness matrix. The encounter of a critical point is signified by the vanishing of both such parameters [7–15].

In direct methods the condition for occurence of a critical point is included in the system of equations to be solved. The solution of the set of extended equations yields directly the position of the critical point and its associated eigenmode together with the load parameter.

Once a critical point has been found a path switching algorithm has to be subsequently applied to follow the deformation of the structure along the possible bifurcation paths [16, 17]. A review of direct and indirect methods and path switching strategies can be found in reference [18].

In this paper a new approach for detecting critical points is proposed. The method is based on the prediction of the *critical displacement* pattern. This is found by writting the tangent stiffness singularity condition at the critical

† *Lecturer on leave from Department of Civil Engineering, University of Brasilia, Brazil*

point using a predicted perturbation of the last converged displacement field. The problem can be posed as a non linear eigenvalue one which can be simply linearized to provide an accurate estimate of the displacement pattern at the critical point. The critical load can be subsequently computed using a secant load–displacement stiffness relationship. The type of critical point (i.e. limit or bifurcation point) can be simply detected by computing the eigenvector corresponding to the (approximate) tangent stiffness matrix at the critical point.

The ideas presented in this paper are a summary of the work reported by the authors in the development of non linear solution procedures based on the secant stiffness matrix [19–22]. The lay–out of the paper is as follows. First some simple concepts of elastic stability analysis are given together with the basic equations of geometrically non linear solid mechanics. Then, the derivation of the secant stiffness matrix, which is an essential ingredient of the approach proposed, is described for three dimensional solids. The critical displacement methodology is then presented in some detail and some alternatives to enhance its computational efficiency are discussed. The accuracy of the new approach is validated with examples of application to the detection of limit and bifurcation points in two and three dimensional truss structures.

2. BASIC IDEAS OF THE CRITICAL DISPLACEMENT METHOD

The approach proposed here is based on the assumption that the critical displacement vector $\mathbf{a}_c$ can be written as

$$\mathbf{a}_c = \mathbf{a}_0 + \Delta\mathbf{a}_c \tag{1}$$

where $\mathbf{a}_0$ is the displacement vector at the known equilibrium configuration P_0. Vector $\Delta\mathbf{a}_c$ is now assumed to be of the form $\Delta\mathbf{a}_c = \lambda\phi$ where ϕ is an estimation of the critical displacement increment pattern. The simplest choice $\phi = \mathbf{a}_0$ can be chosen as shown in the examples given in the paper.

The displacement field (1) can be used to write the tangent stiffness singularity condition at the critical point as the following non linear eigenvalue problem

$$\left|\mathbf{K}_T + \lambda\mathbf{K}_1(\phi) + \lambda^2\mathbf{K}_2(\phi^2)\right| = 0 \tag{2}$$

where $\mathbf{K}_T$ is the tangent stiffness matrix at the known equilibrium configuration P_0 and $\mathbf{K}_1$ and $\mathbf{K}_2$ are linear and quadratic functions of the predicted critical displacement increment pattern, respectively. Eq. (2) can be simplified by neglecting the quadratic terms. Once the mininuum eigenvalue λ is found, the critical displacement vector is obtained as $\mathbf{a}_c = \mathbf{a}_0 + \lambda\phi$.

The value of the critical load vector $\mathbf{f}_c$ can be subsequently computed from the secant load–displacement relationship, i.e.

$$\mathbf{f}_c = \mathbf{K}_S(\mathbf{a}_c^2)\mathbf{a}_c \tag{3}$$

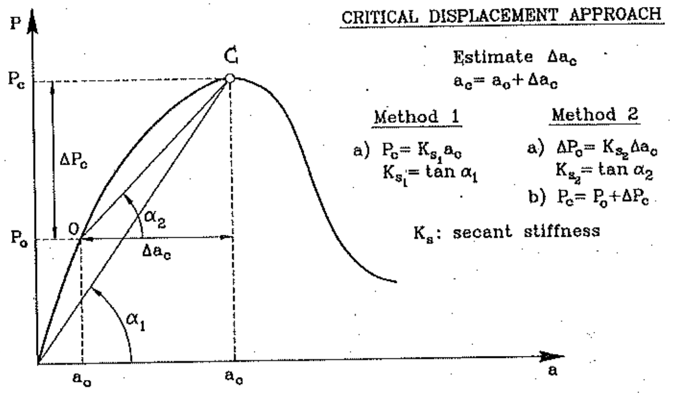

Figure 1. Schematic representation of the critical displacement approach

where $\mathbf{K}_S$ is the secant stiffness matrix which has a quadratic dependence on the nodal displacements [20–22]. This process is schematically shown in Figure 1.

This procedure has proved to give very accurate predictions of both the critical displacement and critical load values even when the initial equilibrium configuration P_0 is taken to correspond with that given by an infinitessimal linear load–displacement relationship. Obviously; the accuracy improves when the initial displacement field $\mathbf{a}_0$ approaches the critical value.

Details of the derivation of the secant stiffness matrix and the critical displacement approach proposed are given in next sections.

3. DERIVATION OF THE SECANT STIFFNESS MATRIX

The potential of using the "exact" form of the secant stiffness matrix for developing new solution algorithms in non linear solid mechanics has been recently recognized by different authors [19–25], [28–32]. One of the problems in using secant stiffness based procedures is that the expression of this matrix is not unique and non symmetrical forms are found unless a careful derivation is performed. Different symmetric expressions of the secant stiffness matrix have been obtained by several authors in the context of the finite element displacement method and a total lagrangian description [33–39]. Alternative symmetric forms based on a mixed formulation were successfully derived and exploited by Kroplin and coworkers [23–25, 30]. Recently Oñate [21] has developed a general methodology for deriving the secant stiffness matrix for geometrically non linear analysis of solids and trusses using a generalized

lagrangian description. This methodology will be followed in this paper and its basic ingredients are given next.

3.1 Basic non Linear Equations

Let us consider a three dimensional body with initial volume ${}^0V$ in equilibrium at a known configuration ${}^tV$ under body forces ${}^t\mathbf{b}$, surface loads ${}^t\mathbf{t}$ and point loads ${}^t\mathbf{p}$. As usual the superscript t denotes a particular time or load level in dynamic or quasistatic analysis, respectively. When the external forces are incremented the body changes its configuration from ${}^tV$ to ${}^{t+\Delta t}V$. The coordinates of the body at each configuration are refered to the global Cartesian system x_1, x_2, x_3. The displacements at $t+\Delta t$ are (in vector form) [40]

$$ {}^{t+\Delta t}\mathbf{u} = {}^t\mathbf{u} + \Delta\mathbf{u} \tag{4} $$

where ${}^t\mathbf{u}$ are the known displacements at time (or load level) t and $\Delta\mathbf{u}$ are the sought displacement increments (see Figure 1).

A *generalized lagrangian* description will be used in which strains and stresses are refered to an intermediate reference configuration ${}^rV$. (Figure 2).

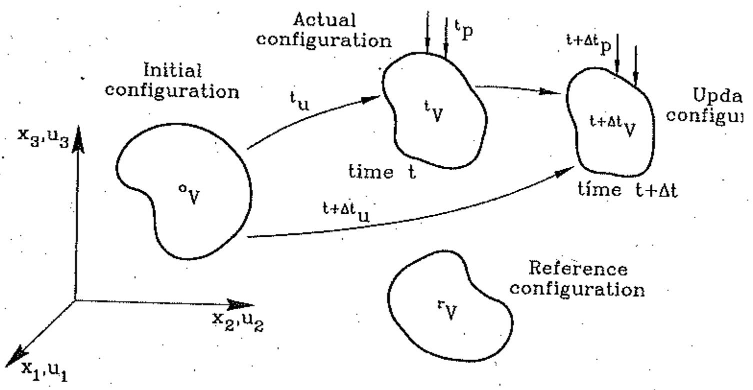

Figure 2. Deformation of a body in a stationary coordinate system

The strain tensor at $t+\Delta t$ refered to the configuration ${}^rV$ can be written as

$$ {}^{t+\Delta t}_{\ \ r}\varepsilon = \frac{1}{2}\left({}^{t+\Delta t}_{\ \ r}u_{i,j} + {}^{t+\Delta t}_{\ \ r}u_{j,i} + {}^{t+\Delta t}_{\ \ r}u_{k,i}\,{}^{t+\Delta t}_{\ \ r}u_{k,j}\right) \tag{5} $$

where

$$ {}^{t+\Delta t}_{r}u_{i,j} = \frac{\partial^{t+\Delta t}u_i}{\partial^r x_j}, \qquad i,j = 1,2,3 \tag{6} $$

The left index in (5) and (6) denotes the configuration to which strains (and stresses) are refered. Note that for ${}^rV = {}^oV$ eq. (5) yields precisely the well known expression of the Green-Lagrange strain tensor in the total lagrangian (TL) description. Also for ${}^rV = {}^tV$ the expression of the linear part of the Almansi strain tensor, typical of the updated lagrangian (UL) formulation can be derived from (5).

The strain increments are obtained as

$$ {}_r\Delta\varepsilon_{ij} = {}^{t+\Delta t}_{r}\varepsilon_{ij} - {}^{t}_{r}\varepsilon_{ij} = {}_re_{ij} + {}_r\eta_{ij} \tag{7} $$

where ${}_re_{ij}$ and ${}_r\eta_{ij}$ are the first and second order strain increments. From (4) and (5) it can be obtained

$$ {}_re_{ij} = \frac{1}{2}\Big({}_r\Delta u_{i,j} + {}_r\Delta u_{j,i} + \underbrace{{}^t_ru_{k,i}\,{}_r\Delta u_{k,j} + {}_r\Delta u_{k,i}\,{}^t_ru_{k,j}}_{=0 \ \text{for} \ {}^rV = {}^tV} \Big) \tag{8a} $$

$$ {}_r\eta_{ij} = \frac{1}{2}\,{}_r\Delta u_{k,i}\ {}_r\Delta u_{k,j} \tag{8b} $$

where

$$ {}_r\Delta u_{i,j} = \frac{\partial(\Delta u_i)}{\partial^r x_j} \qquad i,j = 1,2,3 \tag{9} $$

Eqs. (8a) and (8b) are easily particularized for the TL and UL formulations simply by making $r = 0$ and $r = t$, respectively. Note, that the underlined terms in (8a) are zero in the UL formulation (${}^rV = {}^tV$).

For convenience we will write the first and second order strain increment vectors as

$$ {}_r\mathbf{e} = [\mathbf{L}_0 + {}^t_r\mathbf{L}_1({}^t_r\mathbf{g})]\,{}_r\mathbf{g} \tag{10} $$

$$ {}_r\boldsymbol{\eta} = \frac{1}{2}{}_r\mathbf{L}_1({}_r\mathbf{g})_r\mathbf{g} \tag{11} $$

In above ${}^t_r\mathbf{g}$ and ${}_r\mathbf{g}$ are displacement and displacement increment gradient vectors respectively, $\mathbf{L}_0$ is a rectangular matrix containing ones and zeros and ${}^t_r\mathbf{L}_1$ and ${}_r\mathbf{L}_1$ are displacement and displacement increment dependent matrices, respectively.

For 3D solids

$$ \begin{aligned} {}_r\mathbf{e} &= [\,{}_re_{11},\ {}_re_{22},\ {}_re_{33}, 2\,{}_re_{12}, 2\,{}_re_{13}, 2\,{}_re_{23}]^T \\ {}_r\boldsymbol{\eta} &= [\,{}_r\eta_{11},\ {}_r\eta_{22},\ {}_r\eta_{33}, 2\,{}_r\eta_{12}, 2\,{}_r\eta_{13}, 2\,{}_r\eta_{23}]^T \end{aligned} \tag{12} $$

$$ \mathbf{L}_0 = \begin{bmatrix} 100 & 000 & 000 \\ 000 & 010 & 000 \\ 000 & 000 & 001 \\ 010 & 100 & 000 \\ 001 & 000 & 100 \\ 000 & 001 & 010 \end{bmatrix} \tag{13} $$

$$ {}^t_r\mathbf{L}_1 = \begin{bmatrix} {}^t_r\mathbf{g}^T\mathbf{H}_1 \\ {}^t_r\mathbf{g}^T\mathbf{H}_2 \\ \vdots \\ {}^t_r\mathbf{g}^T\mathbf{H}_6 \end{bmatrix}; \qquad {}_r\mathbf{L}_1 = \begin{bmatrix} {}_r\mathbf{g}^T\mathbf{H}_1 \\ {}_r\mathbf{g}^T\mathbf{H}_2 \\ \vdots \\ {}_r\mathbf{g}^T\mathbf{H}_6 \end{bmatrix} \tag{14} $$

where

$$ {}^t_r\mathbf{g} = \begin{Bmatrix} {}^t_r\mathbf{g}_1 \\ {}^t_r\mathbf{g}_2 \\ {}^t_r\mathbf{g}_3 \end{Bmatrix}; \qquad {}_r\mathbf{g} = \begin{Bmatrix} {}_r\mathbf{g}_1 \\ {}_r\mathbf{g}_2 \\ {}_r\mathbf{g}_3 \end{Bmatrix} \tag{15} $$

with

$$ {}^t_r\mathbf{g}_i = \frac{\partial\,{}^t\mathbf{u}}{\partial\,{}^rx_i}; \qquad {}_r\mathbf{g}_i = \frac{\partial(\Delta\mathbf{u})}{\partial\,{}^rx_i} \tag{16} $$

and

$$ \mathbf{H}_1 = \begin{bmatrix} \mathbf{I}_3 & \mathbf{0} & \mathbf{0} \\ \mathbf{0} & \mathbf{0} & \mathbf{0} \\ \mathbf{0} & \mathbf{0} & \mathbf{0} \end{bmatrix}; \quad \mathbf{H}_2 = \begin{bmatrix} \mathbf{0} & \mathbf{0} & \mathbf{0} \\ \mathbf{0} & \mathbf{I}_3 & \mathbf{0} \\ \mathbf{0} & \mathbf{0} & \mathbf{0} \end{bmatrix} $$

$$ \mathbf{H}_3 = \begin{bmatrix} \mathbf{0} & \mathbf{0} & \mathbf{0} \\ \mathbf{0} & \mathbf{0} & \mathbf{0} \\ \mathbf{0} & \mathbf{0} & \mathbf{I}_3 \end{bmatrix}; \quad \mathbf{H}_4 = \begin{bmatrix} \mathbf{0} & \mathbf{I}_3 & \mathbf{0} \\ \mathbf{I}_3 & \mathbf{0} & \mathbf{0} \\ \mathbf{0} & \mathbf{0} & \mathbf{0} \end{bmatrix} $$

$$ \mathbf{H}_5 = \begin{bmatrix} \mathbf{0} & \mathbf{0} & \mathbf{I}_3 \\ \mathbf{0} & \mathbf{0} & \mathbf{0} \\ \mathbf{I}_3 & \mathbf{0} & \mathbf{0} \end{bmatrix}; \quad \mathbf{H}_6 = \begin{bmatrix} \mathbf{0} & \mathbf{0} & \mathbf{0} \\ \mathbf{0} & \mathbf{0} & \mathbf{I}_3 \\ \mathbf{0} & \mathbf{I}_3 & \mathbf{0} \end{bmatrix} $$

$$ \mathbf{I}_3 = \begin{bmatrix} 1 & 0 & 0 \\ 0 & 1 & 0 \\ 0 & 0 & 1 \end{bmatrix}; \quad \mathbf{0} = \begin{bmatrix} 0 & 0 & 0 \\ 0 & 0 & 0 \\ 0 & 0 & 0 \end{bmatrix} \tag{17} $$

The virtual strains are defined as the first variation of the strains in the configuration ${}^{t+\Delta t}V$. On the other hand, the displacements ${}^tu_i$ can be considered as fixed during the deformation increment and thus $\delta^tu_i = 0$. Taking this into account we can write

$$ \delta^{t+\Delta t}_{\ r}\varepsilon_{ij} = \delta\,{}_re_{ij} + \delta\,{}_r\eta_{ij} \tag{18} $$

where

$$\delta_r e_{ij} = \frac{1}{2}(\delta_r \Delta u_{i,j} + \delta_r \Delta u_{j,i} + \underline{{}^t_r u_{k,i}\,\delta_r \Delta u_{k,j} + \delta_r \Delta u_{k,i}\, {}^t_r u_{k,j}}) \tag{19a}$$

$$\delta_r \eta_{ij} = \frac{1}{2}(\delta_r \Delta u_{k,i}\, {}_r\Delta u_{k,j} + {}_r\Delta u_{k,i}\,\delta_r \Delta u_{k,j}) \tag{19b}$$

with

$$\delta_r \Delta u_{i,j} = \frac{\partial(\delta \Delta u_i)}{\partial\, {}^r x_j}, \qquad i,j = 1,2,3 \tag{20}$$

where $\delta\Delta u_i$ are the virtual displacement increments. Again the underlined terms in (19a) are zero in the UL formulation. In matrix form we can write from (10) and (11)

$$\delta_r \mathbf{e} = (\mathbf{L}_0 + {}^t_r\mathbf{L}_1)\,\delta_r \mathbf{g} \tag{21a}$$

$$\delta_r \boldsymbol{\eta} = {}_r\mathbf{L}_1 \delta_r \mathbf{g} \tag{21b}$$

The linear elastic constitutive equations relating second Piola-Kirchhoff stress increments and Green-Lagrange strain increments can be written as

$${}_r\Delta\boldsymbol{\sigma} = {}^t_r\mathbf{D}\,{}_r\Delta\boldsymbol{\varepsilon} = {}^t_r\mathbf{D}\,({}_r\mathbf{e} + {}_r\boldsymbol{\eta}) \tag{22}$$

where ${}^t_r\mathbf{D}$ is the constitutive matrix in the configuration ${}^tV$ and refered to ${}^rV$. The stresses at $t + \Delta t$ are simply obtained by

$${}^{t+\Delta t}_r\boldsymbol{\sigma} = {}^t_r\boldsymbol{\sigma} + {}_r\Delta\boldsymbol{\sigma} \tag{23}$$

Finally the principle of virtual work (PVW) at ${}^{t+\Delta t}V$ can be written in matrix form as

$$\int_{{}^rV} \delta\, {}^{t+\Delta t}_r\boldsymbol{\varepsilon}^T\, {}^{t+\Delta t}_r\boldsymbol{\sigma}\, dV = \int_{{}^rV} \delta\, {}^{t+\Delta t}\mathbf{u}^T\, {}^{t+\Delta t}\mathbf{b}\, dV \tag{24a}$$

where

$${}^{t+\Delta t}\mathbf{b} = [{}^{t+\Delta t}b_1, {}^{t+\Delta t}b_2, {}^{t+\Delta t}b_3]^T \tag{24b}$$

For simplicity only body forces $\mathbf{b}$ are assumed to act in (24a).

From eqs. (4), (18), (23) and (24) and noting again that $\delta\, {}^t\mathbf{u} = 0$, eq. (24a) can be rewritten as

$$\int_{{}^rV} \Big[\delta_r \mathbf{e}^T\, {}^t_r\mathbf{D}\, {}_r\mathbf{e} + \underline{(\delta_r \mathbf{e}^T\, {}^t_r\mathbf{D}\, {}_r\boldsymbol{\eta} + \delta_r \boldsymbol{\eta}^T\, {}^t_r\mathbf{D}\, {}_r\mathbf{e}) + \delta_r \boldsymbol{\eta}^T\, {}^t_r\mathbf{D}\, {}_r\boldsymbol{\eta}} + {} + \delta_r \boldsymbol{\eta}^T\, {}^t_r\boldsymbol{\sigma}\Big] dV = \int_{{}^rV} \delta\Delta\mathbf{u}^T\, {}^{t+\Delta t}\mathbf{b}\, dV - \int_{{}^rV} \delta_r \mathbf{e}^T\, {}^t_r\boldsymbol{\sigma}\, dV \tag{25}$$

Eq. (25) is the *full incremental form* of the PVW and it is also the basis for obtaining the incremental finite element equations. Note that the right hand side of (25) is independent of the displacement increments and it will lead to the expression of the out of balance or residual forces after discretization. On the other hand, all the terms in the left hand side are a function of the

displacement increments. In particular note that the underlined terms in (25) contain quadratic and cubic expressions of the displacement increments. The consideration of these terms is crutial for the derivation of the secant stiffness matrix. A linearization of eq. (25) will neglect these terms, yielding the standard tangent stiffness matrix. The derivation of these two matrices for elasticity problems is presented in next section.

3.2 Finite Element Discretization. Derivation of the Secant Stiffness Matrix

We will consider a discretization of a general solid in standard 3D isoparametric C° continuous finite elements with n nodes and nodal shape functions $N^k(\xi, \eta, \zeta)$ defined in the natural coordinate system ξ, η, ζ.

The displacement and displacement increment fields within each element are defined by the standard interpolations [40, 41]

$${}^t\mathbf{u} = \mathbf{N}\, {}^t\mathbf{a} \qquad \text{and} \qquad \Delta\mathbf{u} = \mathbf{N}\Delta\mathbf{a} \tag{26}$$

where

$$\mathbf{N} = [\mathbf{N}^1, \mathbf{N}^2, \cdots, \mathbf{N}^n]; \qquad \mathbf{N}^k = N^k \mathbf{I}_3$$

$${}^t\mathbf{a} = \begin{Bmatrix} {}^t\mathbf{a}^1 \\ \vdots \\ {}^t\mathbf{a}^n \end{Bmatrix}; \quad \Delta\mathbf{a} = \begin{Bmatrix} \Delta\mathbf{a}^1 \\ \vdots \\ \Delta\mathbf{a}^n \end{Bmatrix}; \quad \begin{matrix} {}^t\mathbf{a}^k = [{}^tu_1^k, {}^tu_2^k, {}^tu_3^k]^T \\ \Delta\mathbf{a}^k = [\Delta u_1^k, \Delta u_2^k, \Delta u_3^k]^T \end{matrix} \tag{27}$$

are the shape function matrices and the displacement and displacement increment vectors of the element and of a node k, respectively and $\mathbf{I}_3$ is the 3×3 unit matrix.

Substitution of the approximation (26) into (15) allows to express the vector of displacement increment gradients in terms of the nodal displacement increments as

$${}_r\mathbf{g} = {}_r\mathbf{G}\Delta\mathbf{a} \tag{28}$$

Substituting (28) into eqs. (10), (11) and (21) gives

$$\begin{aligned} {}_r\mathbf{e} &= {}^t_r\mathbf{B}_L\Delta\mathbf{a} \quad , \quad & \delta_r\mathbf{e} &= {}^t_r\mathbf{B}_L\delta(\Delta\mathbf{a}) \\ {}_r\boldsymbol{\eta} &= \frac{1}{2}{}_r\mathbf{B}_1\Delta\mathbf{a} \quad , \quad & \delta_r\boldsymbol{\eta} &= {}_r\mathbf{B}_1\delta(\Delta\mathbf{a}) \end{aligned} \tag{29}$$

Matrix ${}^t_r\mathbf{B}_L({}^t\mathbf{a})$ can be splitted as

$${}^t_r\mathbf{B}_L({}^t\mathbf{a}) = {}_r\mathbf{B}_{L_0} + \underline{{}^t_r\mathbf{B}_{L_1}}({}^t\mathbf{a}) \tag{30}$$

where ${}_r\mathbf{B}_{L_0}$ is the standard displacement independent matrix as derived from infinitesimal theory [40, 41] and ${}^t_r\mathbf{B}_{L_1}$ is the displacement-dependent part of the first order strain increment matrix. This matrix vanishes in the case of the UL formulation.

$$ {}_r\mathbf{g} = {}_r\mathbf{G}\Delta\mathbf{a} \quad ; \quad {}_r\mathbf{G}^k = \begin{bmatrix} \dfrac{\partial N^k}{\partial\, {}^r x_1} & \mathbf{I}_3 \\ \dfrac{\partial N^k}{\partial\, {}^r x_2} & \mathbf{I}_3 \\ \dfrac{\partial N^k}{\partial\, {}^r x_3} & \mathbf{I}_3 \end{bmatrix} $$

$$ {}_r\mathbf{e} = {}_r^t\mathbf{B}_L\Delta\mathbf{a} \quad ; \quad {}_r\boldsymbol{\eta} = \frac{1}{2}\,{}_r\mathbf{B}_1\Delta\mathbf{a} $$

$$ {}_r^t\mathbf{B}_L({}^t\mathbf{a}) = {}_r\mathbf{B}_{L_0} + {}_r^t\mathbf{B}_{L_1}({}^t\mathbf{a}) $$

$$ {}_r\mathbf{B}_{L_0}^{k} = \mathbf{L}_0\,{}_r\mathbf{G}^k \quad ; \quad {}_r^t\mathbf{B}_{L_1}^k({}^t\mathbf{a}) = {}_r^t\mathbf{L}_1({}^t\mathbf{a})\,{}_r\mathbf{G}^k \quad ; \quad {}_r\mathbf{B}_1(\Delta\mathbf{a}) = {}_r\mathbf{L}_1(\Delta\mathbf{a})\,{}_r\mathbf{G}^k $$

$$ {}_r^t\mathbf{E} = \begin{bmatrix} a\mathbf{I}_3 & d\mathbf{I}_3 & e\mathbf{I}_3 \\ & b\mathbf{I}_3 & f\mathbf{I}_3 \\ \text{sym.} & & c\mathbf{I}_3 \end{bmatrix} ; \quad [a,b,c,d,e,f]^T = {}_r^t\mathbf{D}\;{}_r\mathbf{e} $$

$$ {}_r\mathbf{B}_{NL} = \begin{bmatrix} {}_r\bar{\mathbf{B}}_{NL} & \bar{0} & \bar{0} \\ \bar{0} & {}_r\bar{\mathbf{B}}_{NL} & \bar{0} \\ \bar{0} & \bar{0} & {}_r\bar{\mathbf{B}}_{NL} \end{bmatrix} ; \; {}_r\bar{\mathbf{B}}_{NL} = \begin{bmatrix} {}_rN^1_{,1} & 0 & 0 & {}_rN^2_{,1} & 0 & 0 & \cdots & {}_rN^n_{,1} \\ {}_rN^1_{,2} & 0 & 0 & {}_rN^2_{,2} & 0 & 0 & \cdots & {}_rN^n_{,2} \\ {}_rN^1_{,3} & 0 & 0 & {}_rN^2_{,3} & 0 & 0 & \cdots & {}_rN^n_{,3} \end{bmatrix} $$

$$ {}_r^t\mathbf{S} = \begin{bmatrix} {}_r^t\bar{\mathbf{S}} & 0 & 0 \\ 0 & {}_r^t\bar{\mathbf{S}} & 0 \\ 0 & 0 & {}_r^t\bar{\mathbf{S}} \end{bmatrix} ; \quad {}_r^t\bar{\mathbf{S}} = \begin{bmatrix} {}_r^t\sigma_{11} & {}_r^t\sigma_{12} & {}_r^t\sigma_{13} \\ {}_r^t\sigma_{12} & {}_r^t\sigma_{22} & {}_r^t\sigma_{23} \\ {}_r^t\sigma_{13} & {}_r^t\sigma_{23} & {}_r^t\sigma_{33} \end{bmatrix} $$

$$ 0 = \begin{bmatrix} 0 & 0 & 0 \\ 0 & 0 & 0 \\ 0 & 0 & 0 \end{bmatrix} ; \quad \bar{0} = \begin{Bmatrix} 0 \\ 0 \\ 0 \end{Bmatrix} ; \quad {}_rN^k_{,i} = \frac{\partial N^k}{\partial\, {}^r x_i} $$

$$ {}_r^t\mathbf{H} = \sum_{i=1}^{6}\sum_{j=1}^{6} {}_r^t d_{ij}\,{}_r\eta_j \mathbf{H}_i ; \quad {}_r\eta_j = {}_r\mathbf{g}^T \mathbf{H}_j\,{}_r\mathbf{g} $$

${}_r^t d_{ij}$: element ij of constitutive matrix ${}_r^t\mathbf{D}$

Box 1. Relevant matrices for 3D elastic solids

The form of all above matrices for the case of 3D solids is given in Box 1. Further details can be found in [21, 22].

The incremental constitutive equations (22) can be written now in terms

of the nodal displacement increments as

$$ {}_r\Delta\boldsymbol{\sigma} = {}_r^t\mathbf{D}\left[{}_r^t\mathbf{B}_L + \frac{1}{2}\,{}_r\mathbf{B}_1\right]\Delta\mathbf{a} \tag{31} $$

Substituting now eqs. (29) and (31) into the PVW expression (25) the following relationship relating the total applied forces with the nodal displacement increments can be obtained

$$ {}_r^t\mathbf{K}_S(\Delta\mathbf{a})\Delta\mathbf{a} = -{}^{t+\Delta t}_{\;\;r}\mathbf{r} \tag{32} $$

In eq. (32) ${}_r^t\mathbf{r}$ is the standard residual force vector which can be written for each element with volume ${}^rV^{(e)}$ as

$$ {}^{t+\Delta t}_{\;\;r}\mathbf{r}^{(e)} = \int_{{}^rV^{(e)}} {}_r^t\mathbf{B}_L^T\,{}_r^t\boldsymbol{\sigma}\,dV - {}^{t+\Delta t}\mathbf{f}^{(e)} \tag{33a} $$

with

$$ {}^{t+\Delta t}\mathbf{f}^{(e)} = \int_{{}^rV^{(e)}} \mathbf{N}\;{}^{t+\Delta t}\mathbf{b}\,dV \tag{33b} $$

being the equivalent nodal force vector for the element, and ${}_r^t\mathbf{K}_S$ is the *incremental secant stiffness matrix* which can be written as

$$ \boxed{{}_r^t\mathbf{K}_S(\Delta\mathbf{a}) = {}_r^t\mathbf{K}_L + {}_r^t\mathbf{K}_M(\Delta\mathbf{a}) + {}_r^t\mathbf{K}_N(\Delta\mathbf{a}^2) + {}_r^t\mathbf{K}_\sigma} \tag{34} $$

where for each element

$$ {}_r^t\mathbf{K}_L = \int_{{}^rV^{(e)}} {}_r^t\mathbf{B}_L^T\,{}_r^t\mathbf{D}\,{}_r^t\mathbf{B}_L\,dV \tag{35a} $$

$$ {}_r^t\mathbf{K}_M(\Delta\mathbf{a}) = \int_{{}^rV^{(e)}} \left[\frac{1}{2}\,{}_r^t\mathbf{B}_L^T\,{}_r^t\mathbf{D}\,{}_r\mathbf{B}_1 + \alpha\,{}_r\mathbf{B}_1^T\,{}_r^t\mathbf{D}\,{}_r^t\mathbf{B}_L + \right. $$
$$ \left. + (1-\alpha)\,{}_r\mathbf{G}^T\,{}_r^t\mathbf{E}\,{}_r\mathbf{G}\right] dV \tag{35b} $$

$$ {}_r^t\mathbf{K}_N(\Delta\mathbf{a}^2) = \int_{{}^rV^{(e)}} \left[\frac{1}{4}(2-\beta)\,{}_r\mathbf{B}_1^T\,{}_r^t\mathbf{D}\,{}_r\mathbf{B}_1 + \frac{\beta}{4}\,{}_r\mathbf{G}^T\,{}_r^t\mathbf{H}\,{}_r\mathbf{G}\right] dV \tag{35c} $$

$$ {}_r^t\mathbf{K}_\sigma = \int_{{}^rV^{(e)}} {}_r\mathbf{B}_{NL}^T\,{}_r^t\mathbf{S}\,{}_r\mathbf{B}_{NL}\,dV \tag{35d} $$

The global secant stiffness matrix and the residual force vector for the whole structure are assembled from the individual element contributions in the standard manner [40, 41].

The form of the different matrices appearing in eqs. (35) is given in Box 1 for the case of 3D solids. Further details can be found in [21].

The parametric expression of the incremental secant stiffness matrix as given above has been recently derived by Oñate [21]. Note that this expression is non symmetric for values of $\alpha \neq 1/2$. An infinite set of symmetric forms is obtained for $\alpha = 1/2$ depending on the values of the parameter β. The particular symmetric expression of the incremental secant stiffness matrix for $\alpha = 1/2$, $\beta = 0$ was also derived by Oñate in a previous work [20]. A similar parametric form of the secant stiffness matrix was derived by Felippa and co-workers [36, 37] using a TL description.

4. ITERATIVE SOLUTION TECHNIQUES

Eq. (32) can be used to solve for the new equilibrium configuration at $t+\Delta t$ by means of an *incremental secant* approach (Figure 3a) giving

$$\Delta \mathbf{a}^i = -\left[{}^t_r\mathbf{K}_S({}^{t+\Delta t}\mathbf{a}^i,\ \Delta\mathbf{a}^{i-1})\right]^{-1}\ {}^{t+\Delta t}_{\ \ r}\mathbf{r}^i \tag{36a}$$

$${}^{t+\Delta t}\mathbf{a}^{i+1} = {}^{t+\Delta t}\mathbf{a}^i + \Delta\mathbf{a}^i \tag{36b}$$

with ${}^{t+\Delta t}\mathbf{a}^0 = {}^t\mathbf{a}$ and $\Delta\mathbf{a}^{-1} = \mathbf{0}$. Convergence of the iteration process is controlled by the satisfaction of an adequate norm in the nodal displacement increments or the residual force vector [40, 41].

A particular case of above procedure corresponds to that with the residual force vector kept constant during the iterations. This can be simply interpreted as the satisfaction of the following incremental load–displacement relationship (Figure 3b)

$${}^t_r\mathbf{K}_S(\Delta\mathbf{a})\Delta\mathbf{a} = \Delta\mathbf{f} \tag{37}$$

The iterative process reads now simply

$$\Delta\mathbf{a}^{i+1} = \left[{}^t_r\mathbf{K}_S(\Delta\mathbf{a}^i)\right]^{-1}\Delta\mathbf{f} \tag{38}$$

Once convergence is achieved the new equilibrium configuration is simply found as ${}^{t+\Delta t}\mathbf{a} = {}^t\mathbf{a} + \Delta\mathbf{a}^n$ where $\Delta\mathbf{a}^n$ is the last nodal displacement increment vector computed in (38).

The secant expression (37) also holds when the external loads are applied in a single step on the initial load-free configurations (i.e. $t=0$). Now the load and displacement increments in eq. (37) are in fact "total" values and the same iterative process of eq. (38) can be used to find the total displacement vector in a direct manner [21]. Note that in this case matrix ${}^t_r\mathbf{K}_\sigma$ does not contribute to the secant stiffness matrix since the stresses are zero in the load-free configuration.

5. DERIVATION OF THE TANGENT STIFFNESS MATRIX

The expression of the tangent stiffness matrix can be simply obtained as the limit of the incremental secant matrix when the values of the displacement increments tend to zero. Thus from eq. (34) we can write

$${}^t_r\mathbf{K}_T = \lim_{\Delta \mathbf{a}\to 0} {}^t_r\mathbf{K}_S = {}^t_r\mathbf{K}_L + {}^t_r\mathbf{K}_\sigma \tag{39}$$

Note that the resulting tangent stiffness matrix coincides with the standard expression obtained by linearizing the PVW in (25).

For subsequent purposes it is useful to rewrite matrix ${}^t_r\mathbf{K}_L$ using (30) as

$${}^t_r\mathbf{K}_L({}^t\mathbf{a}) = {}^t_r\mathbf{K}_{L_0} + {}^t_r\mathbf{K}_{L_1}({}^t\mathbf{a}) \tag{40a}$$

where

$${}^t_r\mathbf{K}_{L_0} = \int_{^rV^{(e)}} {}_r\mathbf{B}^T_{L_0}\,{}^t_r\mathbf{D}_r\mathbf{B}_{L_0}dV \tag{40b}$$

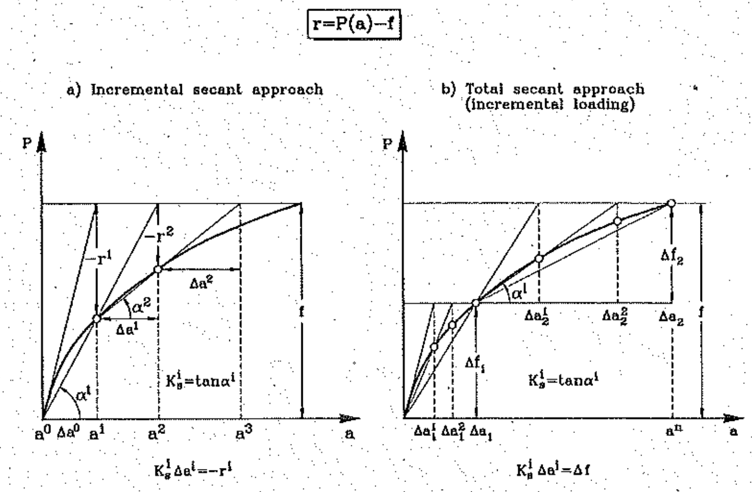

Figure 3. Different secant iterative techniques

is the standard stiffness matrix from infinitessimal elasticity theory and

$${}^t_r\mathbf{K}_{L_1}({}^t\mathbf{a}) = \int_{^rV^{(e)}} \left({}_r\mathbf{B}^T_{L_0}\,{}^t_r\mathbf{D}\,{}^t_r\mathbf{B}_{L_1} + {}^t_r\mathbf{B}_{L_1}\,{}^t_r\mathbf{D}_r\mathbf{B}_{L_0} + {}^t_r\mathbf{B}_{L_1}\,{}^t_r\mathbf{D}\,{}^t_r\mathbf{B}_{L_1}\right) dV \tag{40c}$$

is the so called initial displacement stiffness matrix [40, 41]. An alternative expression of this matrix can be found in [21].

Note finally that the expression of the secant matrix (39) can be rewritten as

$${}^t_r\mathbf{K}_S = {}^t_r\mathbf{K}_T + {}^t_r\mathbf{K}_M + {}^t_r\mathbf{K}_N \tag{41}$$

6. ESTIMATES FOR LIMIT AND BIFURCATION POINTS. CRITICAL DISPLACEMENT APPROACH

A useful application of the concept of secant stiffness matrix is the estimation of the load level originating structural instability (i.e. limit or bifurcation points). These points are characterized by the singularity of the tangent stiffness matrix ${}^t_r\mathbf{K}_T$. The approach proposed here is based in the estimation of the *critical displacement values* giving singularity of ${}^t_r\mathbf{K}_T$, instead of those of forces as done in classical limit load theory. The secant stiffness relationship is then used to find the critical loading in terms of the critical displacement values in a straightforward manner. Details of this procedure are given next.

The process starts with the prediction of the displacement vector in the critical state as

$$ {}^{t+\Delta t_c}\mathbf{a} = {}^t\mathbf{a} + \Delta\mathbf{a}_c \tag{42} $$

where ${}^t\mathbf{a}$ is the displacement vector at the known equilibrium configuration ${}^tV$ and $\Delta\mathbf{a}_c$ is an estimate of the critical displacement increment yielding structural instability at $t_c = t + \Delta t_c$. Vector $\Delta\mathbf{a}_c$ is now written as $\Delta\mathbf{a}_c = \lambda\boldsymbol{\phi}$ where λ is a multiplier and $\boldsymbol{\phi}$ is an estimate of the buckling pattern at the instability point. Here $\boldsymbol{\phi} = {}^t\mathbf{a}$, $\boldsymbol{\phi}$ equal to the first eigenmode in ${}^t\mathbf{a}$ or $\boldsymbol{\phi} = \Delta\mathbf{a} = {}^t\mathbf{a} - {}^{t-\Delta t}\mathbf{a}$ can be chosen as estimates of the critical displacement increment vector.

With these assumptions the stress field at the critical point can be written as (using eqs. (22, 23, 31 and 42)

$$ {}^{t_c}\boldsymbol{\sigma} = {}^t\boldsymbol{\sigma} + {}^t_r\mathbf{D}\left[{}^t_r\mathbf{B}_L({}^t\mathbf{a}) + \frac{\lambda}{2}\,{}_r\bar{\mathbf{B}}_1(\boldsymbol{\phi})\right]\lambda\boldsymbol{\phi} = {}^t\boldsymbol{\sigma} + \lambda\boldsymbol{\sigma}_1 + \lambda^2\boldsymbol{\sigma}_2 \tag{43a} $$

where

$$ \boldsymbol{\sigma}_1 = {}^t_r\mathbf{D}\,{}^t_r\mathbf{B}_L({}^t\mathbf{a})\boldsymbol{\phi} \tag{43b} $$

$$ \boldsymbol{\sigma}_2 = \frac{1}{2}{}^t_r\mathbf{D}\,{}_r\bar{\mathbf{B}}_1(\boldsymbol{\phi})\boldsymbol{\phi} \tag{43c} $$

Substituting eq. (42) into (30) allows to write the first order strain matrix at the critical point as

$$ {}^{t_c}_r\mathbf{B}_L = {}_r\mathbf{B}_{L_0} + {}^t_r\mathbf{B}_{L_1}({}^t\mathbf{a}) + \lambda\,{}_r\bar{\mathbf{B}}_1(\boldsymbol{\phi}) = {}^t_r\mathbf{B}_L({}^t\mathbf{a}) + \lambda\,{}_r\bar{\mathbf{B}}_1(\boldsymbol{\phi}) \tag{44} $$

In eqs. (42)- (44) ${}_r\bar{\mathbf{B}}_1(\boldsymbol{\phi})$ is obtained from the expression of ${}_r\mathbf{B}_1$ of Box 1 simply substituting $\Delta\mathbf{a}$ by the known predicted increment displacement pattern $\boldsymbol{\phi}$. Note that when $\boldsymbol{\phi} = {}^t\mathbf{a}$ then ${}_r\bar{\mathbf{B}}_1 = {}^t_r\mathbf{B}_{L_1}$.

The tangent stiffness matrix can be written at the critical point taking into account eqs. (39), (40), (43) and (44) as

$$ {}^{t_c}_t\mathbf{K}_T = {}^t_r\mathbf{K}_T + \lambda\left({}^t_r\mathbf{K}_{L_2} + {}^t_r\mathbf{K}_{\sigma_1}\right) + \lambda^2\left({}^t_r\mathbf{K}_{L_3} + {}^t_r\mathbf{K}_{\sigma_2}\right) \tag{45} $$

where ${}^t_r\mathbf{K}_T$ is the tangent stiffness matrix at the known equilibrium configuration ${}^tV$ and

$$ {}^t_r\mathbf{K}_{L_2} = \int_{{}^rV^{(e)}}\left[{}^t_r\mathbf{B}_L^T\,{}^t_r\mathbf{D}_r\bar{\mathbf{B}}_1 + {}_r\bar{\mathbf{B}}_1^T\,{}^t_r\mathbf{D}\,{}^t_r\mathbf{B}_L\right]dV \tag{46a} $$

$$ {}^t_r\mathbf{K}_{L_3} = \int_{{}^rV^{(e)}}{}_r\bar{\mathbf{B}}_1^T\,{}^t_r\mathbf{D}_r\bar{\mathbf{B}}_1\,dV \tag{46b} $$

$$ {}^t_r\mathbf{K}_{\sigma_1} = \int_{{}^rV^{(e)}}{}_r\bar{\mathbf{B}}_{NL}^T\,{}^t_r\mathbf{S}_{1\,r}\bar{\mathbf{B}}_{NL}\,dV \tag{46c} $$

$$ {}^t_r\mathbf{K}_{\sigma_2} = \int_{{}^rV^{(e)}}{}_r\bar{\mathbf{B}}_{NL}^T\,{}^t_r\mathbf{S}_{2\,r}\bar{\mathbf{B}}_{NL}\,dV \tag{46d} $$

where ${}^t_r\mathbf{S}_1$ and ${}^t_r\mathbf{S}_2$ are obtained by substituting the "stresses" $\boldsymbol{\sigma}_1$ and $\boldsymbol{\sigma}_2$ given by (43b) and (43c) into matrix ${}^t_r\mathbf{S}$ of eq. (35d), respectively (see also Box 1).

The condition $|{}^{t_c}_r\mathbf{K}_T| = 0$ yields a quadratic eigenvalue problem which can be solved for the minimum value of λ, thus giving an approximation of the critical displacement by ${}^{t_c}\mathbf{a} = {}^t\mathbf{a} + \lambda\boldsymbol{\phi}$. Obviously, this process can be simplifield by neglecting the quadratic terms in (45). The standard linear eigenvalue problem to be solved now reads simply

$$ \left|{}^t_r\mathbf{K}_T + \lambda\left({}^t_r\mathbf{K}_{L_2} + {}^t_r\mathbf{K}_{\sigma_1}\right)\right| = 0 \tag{47} $$

The critical load increment can be subsequently estimated from the incremental secant relationship (38) as

$$ \Delta\mathbf{f}_c = {}^t_r\mathbf{K}_S(\lambda\boldsymbol{\phi})\lambda\boldsymbol{\phi} = \left[{}^t_r\mathbf{K}_T({}^t\mathbf{a}) + {}^t_r\mathbf{K}_M(\lambda\boldsymbol{\phi}) + {}^t_r\mathbf{K}_N(\lambda^2\boldsymbol{\phi}^2)\right]\lambda\boldsymbol{\phi} \tag{48} $$

where the expression of all matrices coincides with that given in eqs. (35) and (39).

The estimated critical load vector is finally obtained as

$$ {}^{t_c}\mathbf{f} = {}^t\mathbf{f} + \Delta\bar{\mathbf{f}}_c \tag{49} $$

where $\Delta\bar{\mathbf{f}}_c$ is the projection of $\Delta\mathbf{f}_c$ computed from (48) in the direction of the nodal load vector, i.e. after elliminating the spureous contributions associated to nodal load components not included in ${}^t\mathbf{f}$.

Obviously the critical load vector can be computed in a single step from the total secant expression ${}^{t_c}\mathbf{f} = {}^t_r\mathbf{K}_S({}^{t_c}\mathbf{a}){}^{t_c}\mathbf{a}$ (see Figure 1). However the incremental procedure described above has proved to be more accurate in practice.

7. COMPUTATIONAL STRATEGIES

The approach proposed above can be applied in different ways so as to obtain different approximations to the critical load value.

Method I. One step prediction

1) Compute the displacement vector ${}^0\mathbf{a}$ for a small value of the external forces so that infinitessimal theory still holds.
2) Take $\boldsymbol{\phi} = {}^0\mathbf{a}$ as the estimate of the critical displacement increment pattern.
3) Solve the linear eigenvalue problem (47) for the smallest non zero eigenvalue.
4) Estimate the critical load by eqs. (48) and (49).

This process is comparable in cost to the standard "initial" stability problem in struts, plates, shells etc, based in the solution of the eigenvalue problem [40, 41]

$$ \left|{}^t_r\mathbf{K}_{L_0} + \lambda\,{}^t_r\mathbf{K}_\sigma\right| = 0 \tag{50} $$

where the smallest non zero eigenvalue defines the increasing factor of the initial loading ${}^0\mathbf{f}$ to give the so called "buckling" load as $\lambda^0\mathbf{f}$. However, it is well known that in many problems this "initial stability" load can be considerably larger than the actual limit or bifurcation load. The one step "critical displacement" approach proposed here has proved to give a much accurate prediction of the critical load as shown in the examples presented in next section.

Method II. Incremental prediction

1) Compute the displacement vector ${}^t\mathbf{a}$ for each load level ${}^t\mathbf{f}$ in the standard incremental manner.
2) Take $\phi = {}^t\mathbf{a}$ as the estimate of the critical displacement increment pattern.
3) and 4) as in Method I.

This approach differs from the previous one in that the critical load is estimated each time that a new displacement configuration ${}^t\mathbf{a}$ is found. Naturally a standard stability computation can be also performed at each equilibrium configuration. This implies the solution of the eigenvalue problem

$$\left| {}^t_r\mathbf{K}_L + \lambda^t_r {}^t_r\mathbf{K}_\sigma \right| = 0 \tag{51}$$

and the stability load is subsequently computed as $\lambda^t\mathbf{f}$.

Obviously, the values of the critical load estimaled by the two procedures should converge to the "exact" value as the solution approaches the instability configuration. The examples analyzed show that the values of the critical load predicted by the critical displacement approach here proposed are in all cases much accurate than those given by the standard stability method.

Method III. Enhanced incremental prediction

1) Compute the displacement vector ${}^0\mathbf{a}$ corresponding to an initial load level ${}^0\mathbf{f}$ in the standard incremental manner (Here ${}^0\mathbf{f}$ can be taken small enough so as to give initial displacements within the infinitessimal theory range).
2) Take $\phi = {}^0\mathbf{a}$ as the estimate of the critical displacement increment pattern.
3) and 4) as in Method I.
5) Compute the stresses, the residual force vector ${}^{t_c}_r\mathbf{r}$ and the critical load ${}^{t_c}\mathbf{f}$ corresponding to the predicted critical displacement ${}^{t_c}\mathbf{a} = (1+\lambda)^0\mathbf{a}$ using eqs. (33a), (48) and (49).
The fact that the critical displacement values predicted are close to an equilibrium configuration corresponding to a load level ${}^{t_c}\mathbf{f}$ is now exploited as described next.
6) Perform an equilibrium iteration to find corrected values of the predicted critical displacement ${}^{t_c}\mathbf{a}$ *in equilibrium* with the external loads ${}^{t_c}\mathbf{f}$. For this purpose the standard Newton-Raphson technique can be used as

$$\Delta\mathbf{a}^n = -\left[{}^{t_c}_r\mathbf{K}^n_T\right]^{-1} {}^{t_c}_r\mathbf{r}^n \tag{52a}$$

$${}^{t_c}\mathbf{a}^{n+1} = {}^{t_c}\mathbf{a}^n + \Delta\mathbf{a}^n \tag{52b}$$

with

$${}^{t_c}\mathbf{a}^0 = {}^{t_c}\mathbf{a} \tag{53}$$

7) Restart the process from 2) taking $\phi = {}^{t_c}\mathbf{a}$, where ${}^{t_c}\mathbf{a}$ is the converged displacement vector from 6).

This method allows to compute very accurate critical loads in two or three steps as shown in the examples presented next.

8. PARTICULARIZATION FOR STABILITY ANALYSIS OF TRUSSES

Figure 4 displays a typical two node truss element defined in a three dimensional system with global and local axes denoted by x_i and x'_i $(i = 1.3)$ respectively.

For the sake of preciseness an updated lagrangian formulation will be used $({}^rV = {}^tV)$. The first and second order axial strain increments are defined as

$${}_te'_{11} = \frac{d(\Delta u'_1)}{d\,{}^tx'_1}; \quad {}_t\eta'_{11} = \frac{1}{2}\frac{d(\Delta u'_1)}{d^tx'_1}\frac{d(\Delta u'_1)}{d^tx'_1} \tag{54}$$

where $\Delta u'_1$ is the displacement increment along the local axis ${}^tx'_1$.

The constitutive equation is simply

$${}_t\Delta N = {}^t[EA][{}_te'_{11} + {}_t\eta'_{11}] \tag{55}$$

where ${}_t\Delta N$ is the axial force increment and E and A are respectively the Young's modulus and the area of the transverse cross section.

Local and global displacements are related by the standard transformation

$$\Delta u'_j = \frac{\partial\,{}^tx_i}{\partial\,{}^tx'_j}\Delta u_i; \quad i,j = 1,2,3 \tag{56}$$

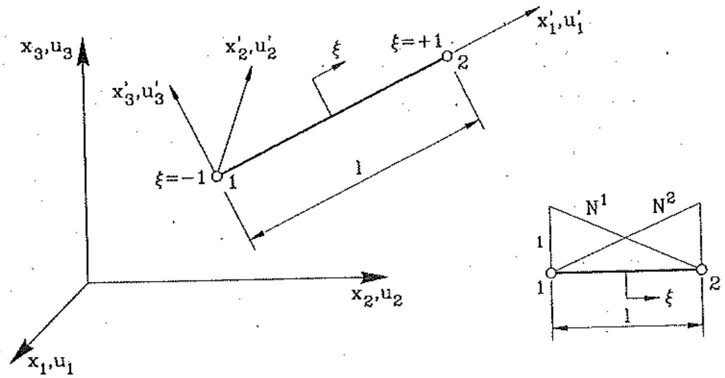

Figure 4. Geometrical description of 3D truss element

The global displacements are interpolated in the usual manner

$$\Delta u_i = \sum_{k=1}^{2} N^k(\xi)\Delta u_i^k \tag{57}$$

where $N^k(\xi) = \frac{1}{2}(1+\xi\xi_k)$ are the linear shape functions of the standard two node element [41].

The expressions of the relevant matrices required for the computation of the secant stiffness matrix are given in Box 2. The particular explicit symmetric form of this matrix for $\alpha = 1/2$ and $\beta = 0$ and a truss of constant cross section and homogeneous material is shown in Box 3.

$$ {}^t_t\mathbf{B}_L = \frac{1}{{}^tj^2}{}^t\mathbf{x}^T\mathbf{N}_{,\xi}^T\,\mathbf{N}_{,\xi} \quad , \quad {}_t\mathbf{B}_1 = \frac{1}{{}^tj^2}\Delta\mathbf{a}^T\,\mathbf{N}_{,\xi}^T\,\mathbf{N}_{,\xi}$$

$$ {}_t\mathbf{B}_{NL} = {}_t\mathbf{G} = \frac{1}{{}^tj}\mathbf{N}_{,\xi} \quad , \quad {}^t_t\mathbf{E} = \frac{{}^t[EA]}{{}^tj^2}{}^t\mathbf{x}^T\mathbf{N}_{,\xi}^T\,\mathbf{N}_{,\xi}\Delta\mathbf{a}$$

$$\mathbf{N}_{,\xi} = \left[\frac{dN^1}{d\xi}\,\mathbf{I}_3,\ \frac{dN^2}{d\xi}\,\mathbf{I}_3\right]; \qquad {}^tj = \frac{d\,{}^tx_1'}{d\xi}\ (\text{usually } {}^tj = \frac{{}^tl^{(e)}}{2})$$

$$ {}^t_t\mathbf{H} = \Delta\mathbf{a}^T\,{}_t\mathbf{G}^T\,{}^t[EA]\,{}_t\mathbf{G}\Delta\mathbf{a}$$

$$ {}^t\mathbf{x} = \left[{}^tx_1^1,\ {}^tx_2^1,\ {}^tx_3^1,\ {}^tx_1^2,\ {}^tx_2^2,\ {}^tx_3^2\right]^T$$

$$\Delta\mathbf{a} = \left[\Delta u_1^1,\ \Delta u_2^1,\ \Delta u_3^1,\ \Delta u_1^2,\ \Delta u_2^2,\ \Delta u_3^2\right]^T$$

Box 2. Relevant expressions for computation of the secant stiffness matrix for linear 3D truss elements

9. EXAMPLES

9.1 2D truss beam

Figure 5 shows the geometry of this example taken from [42]. The beam, formed by truss elements, is subjected to an increasing horizontal load acting at its left end, as shown in the figure.

The critical load path has been predicted using method III proposed in Section 7(eqs. (52) and (53)). The resulting curve obtained (AC) is plotted in Figure 5 where the load path predicted using standard limit load analysis is plotted in curve BC in the same figure. Note the accurary of the predictions based on the critical displacement approach here proposed giving less than 34 % error in the first critical load value predicted from a simple initial infinitesimal solution. This error is reduced to 0.58 % in only three steps as shown in Table I.

$$ {}^t_t\mathbf{K}_{L_{ij}} = {}^t\left[\frac{EA}{l^3}\right](-1)^{i+j}\begin{bmatrix} {}^t(x_{12})^2 & {}^tx_{12}\,{}^ty_{12} & {}^tx_{12}\,{}^tz_{12} \\ & {}^t(y_{12})^2 & {}^ty_{12}\,{}^tz_{12} \\ \text{sym.} & & {}^t(z_{12})^2 \end{bmatrix}$$

$$ {}^t_t\mathbf{K}_{M_{ij}} = {}^t\left[\frac{EA}{2l^3}\right](-1)^{i+j}\begin{bmatrix} 2\,{}^tx_{12}u_{12} & ({}^tx_{12}v_{12}+{}^ty_{12}u_{12}) & ({}^tx_{12}w_{12}+{}^tz_{12}u_{12}) \\ & 2\,{}^ty_{12}v_{12} & ({}^ty_{12}w_{12}+{}^tz_{12}v_{12}) \\ \text{sym.} & & 2\,{}^tz_{12}w_{12} \end{bmatrix}$$

$$ + {}^t\left[\frac{EA}{2l^3}\right](-1)^{i+j}\left[{}^tx_{12}u_{12}+{}^ty_{12}v_{12}+{}^tz_{12}w_{12})\right]\mathbf{I}_3$$

$$ {}^t_t\mathbf{K}_{N_{ij}} = {}^t\left[\frac{EA}{2l^3}\right](-1)^{i+j}\begin{bmatrix} (u_{12})^2 & u_{12}v_{12} & u_{12}w_{12} \\ & (v_{12})^2 & v_{12}w_{12} \\ \text{sym.} & & (w_{12})^2 \end{bmatrix}$$

$$ {}^t_t\mathbf{K}_{\sigma_{ij}} = {}^t\left[\frac{N}{l}\right](-1)^{i+j}\mathbf{I}_3$$

$$ {}^tx_{12} = {}^tx_1 - {}^tx_2, \quad u_{12} = \Delta u_1 - \Delta u_2 \quad \text{etc.} \quad \mathbf{I}_3 = \begin{bmatrix} 1 & 0 & 0 \\ 0 & 1 & 0 \\ 0 & 0 & 1 \end{bmatrix}$$

Box 3. Matrices involved in the expression of the secant stiffness matrix for the two node 3D truss element ($\alpha = 1/2$, $\beta = 0$)

	Critical Displacement Approach		Limit Load Analysis
Load Step	$(u_C)_1$	P_C	P_C
1	6.05 (17.58 %)	3.52×10^5 (34.24 %)	9.85×10^5 (275.26 %)
2	5.83 5.88×10^5 (124.03 %)		
3	5.00 (2.84 %)	2.617×10^5 (0.34 %)	3.52×10^5 (34.00 %)

Table I. 2D truss beam Critical displacement u_c of node 1 and critical load P_c obtained using the critical displacement approach and standard limit load analysis. Numbers in brackets show percentage error with respect to the "exact" solution: $u_c = 5.146$ and $P_c = 2.626 \times 10^{-5}$ [42]

The primary equilibrium path showing snap-back behaviour has been obtained by combining the standard Newton-Raphson incremental procedure with arc-length control.

9.2 3D pin-jointed star dome structures. Limit load analysis

The geometry and material properties of the 3D pin-jointed star dome structure analyzed first is shown in Figure 6. A vertical point load acting on

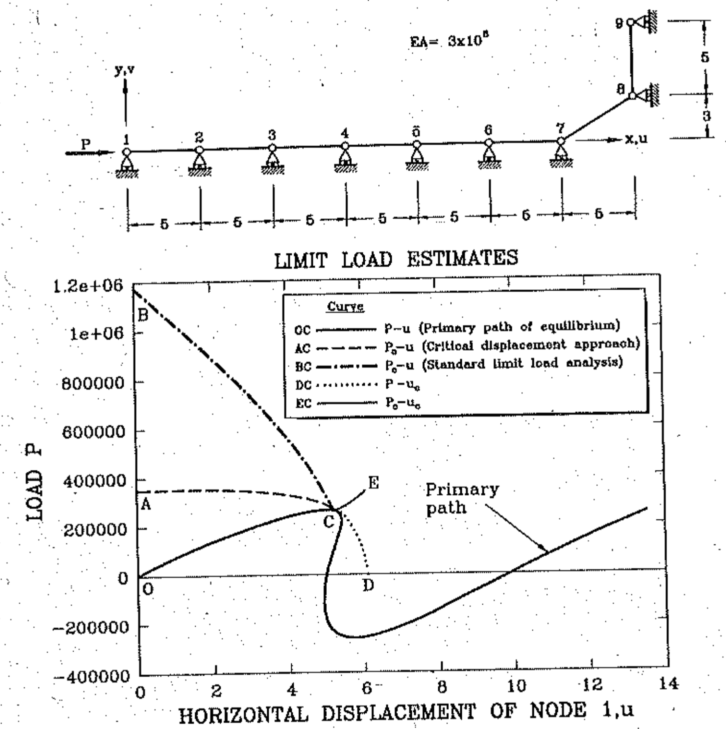

Figure 5. 2D truss beam. Geometry, load–displacement curve and limit load estimates

node 1 is first considered [43].

Figure 6 displays the limit load paths predicted using the critical displacement approach proposed (curve AE) and standard limit load analysis (curve BC). The greater accurary of the predictions based on the new approach, giving 14.82 % error in the first predicted value based on a simple infinitesimal solution, is obvious in this case. This error is reduced to 1.92 % in three steps (see Table II).

9.3 3D pin-jointed truss dome. Prediction of bifurcation load

This example shown the ability of the approach to predict the bifurcation load in a 3D truss structure [18]. The geometry, loading and material properties of the structure are displayed in Figure 7a. The critical load paths obtained with the critical displacement procedure (curve AC) and standard limit load analysis (curve BC) are shown in Figure 7b. A bifurcation point is detected by both procedures for ($P = 26.89$). Note the higher accuracy of the prediction based in the critical displacement procedure. The first estimate of the critical load based on the simple infinitesimal solution gives 19.21 % error. This error is reduced to 2.16 % in only three steps (see Table III).

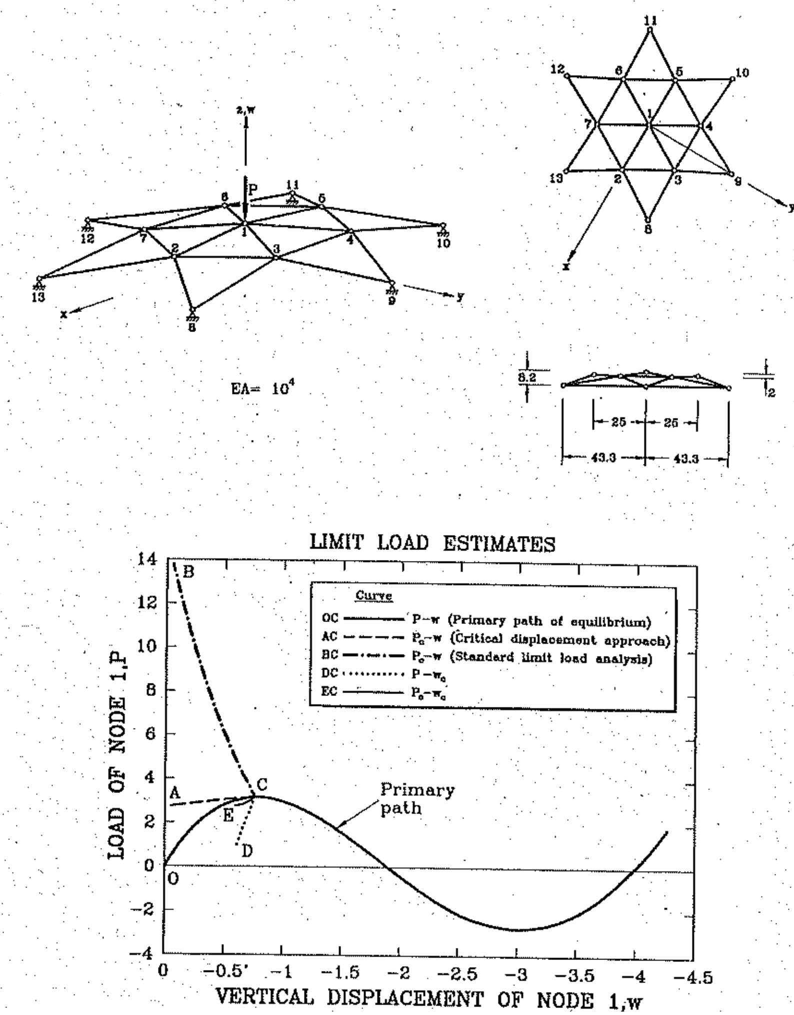

Figure 6. 3D pin–jointed star under central point load. Geometry, load–displacement curve and limit load estimates

The antisymmetric bifurcation path is plotted in curve CD of Figure 7b. This has been obtained by perturbing the geometry of the structure at the critical load using the first eigenmode for this load level and then using an arc length technique.

	Critical Displacement Approach		Limit Load Analysis
Load Step	$(w_C)_1$	P_C	P_C
1	-0.405 (28.25 %)	69.46 (12.94 %)	365.37 (357.95 %)
2	-0.540 (4.42 %)	77.02 (3.46 %)	135.74 (70.14 %)
3	-0.556 (1.51 %)	79.02 (0.95 %)	91.37 (14.52 %)

Table II. 13 node star truss dome under central point load. Critical displacement (w_c) of node 1 and critical load obtained using the critical displacement approach and standard limit load analysis. Number in brackets show porcentage error with respect to the exact solution: $w_c = -0.516$ and $P_c = 79.50$ [43]

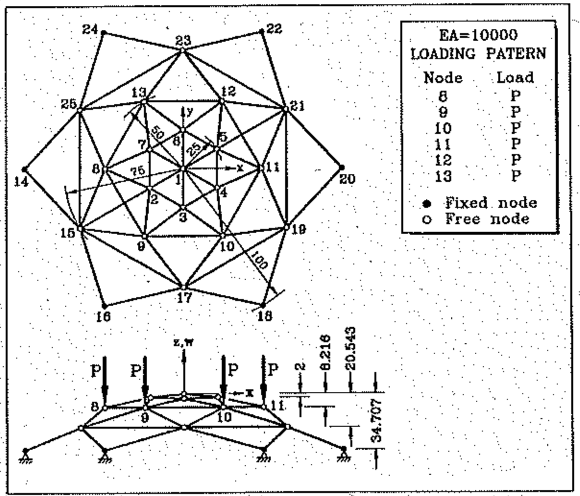

Figure 7a. 25 node star truss dome. Definition of geometry and loading

9.4 Clamped shallow arch

The next two examples show the ability of the formulation to solve bending type instability problems using *solid elements*. The first example is the analysis of a shallow arch clamped at its edges under central vertical load [47,48]. The

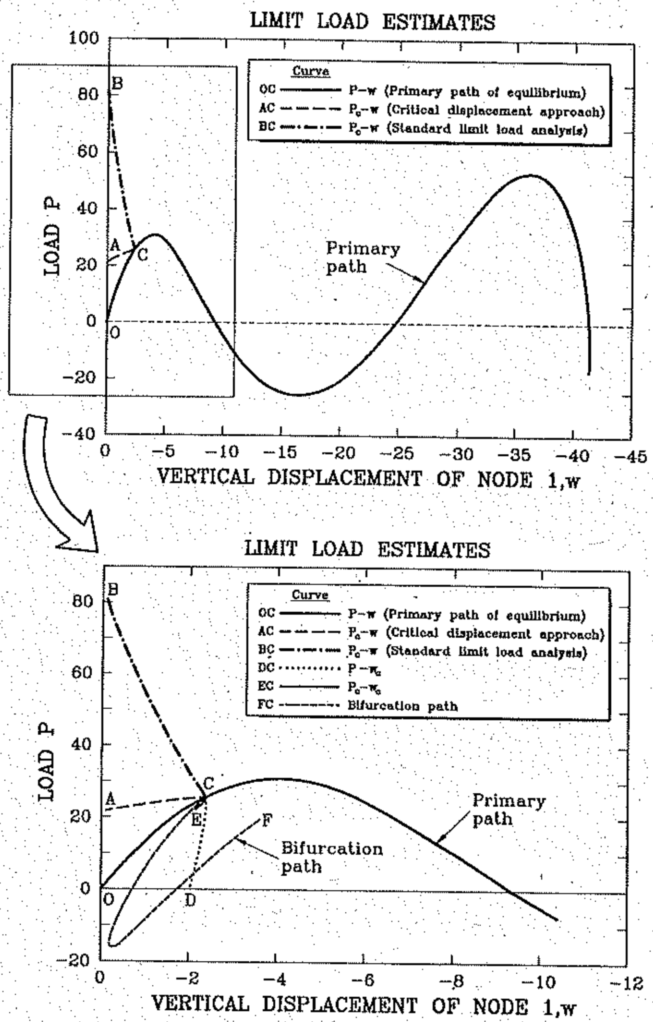

Figure 7b. 25 node star truss dome. Load–displacement curve and limit load estimates

	Critical Displacement Approach		Limit Load Analysis
Load Step	$(w_C)_1$	P_C	P_C
1	-2.05 (18.23 %)	21.71 (19.21 %)	79.79 (196.90 %)
2	-2.37 (5.44 %)	25.39 (5.72 %)	33.35 (24.10 %)
3	-2.42 (3.80 %)	26.69 (2.16 %)	24.92 (7.27 %)

Table III. 25 node star truss dome under four point loads. Critical (bifurcation) load obtained using the critical displacement approach and standard limit load analysis. Number in brackets show porcentage error with respect to the exact solution: $w_c = -2.516$ and $P_c = 26.89$ [19]

geometry and material properties can be seen in Figure 8. 10 standard eight node isoparametric quadrilateral elements with 2×2 integration [41] have been used for the analysis. The different limit load-displacement paths predicted using the critical displacement (CD) approach (curve AE) and standard limit load analysis are shown in the same figure. Note the accuracy of the predictions obtained with the CD method proposed.

9.5 Cylindrical shell

The last example is the stability analysis of a thin cylindrical shell under a central point load [49]. The geometry and material properties are shown in Figure 9. 16 twenty node isoparametric hexahedra with 2 × 2 × 2 integration [41] have been used as shown in the figure. The limit load-displacement paths obtained for this case are also shown in Figure 9.

Note again the higher accuracy of the critical displacement solution versus standard limit load analysis.

CONCLUSIONS

The critical displacement (CD) approach proposed seems to be a simple and effective procedure for computing structural instability points. The cost of the computation is comparable to that of standard stability analysis and the accuracy has proved to be superior in all cases studied. The extension of the CD approach to structural problems involving rotational degrees of freedom (i.e. beams and shells) requires further study as the derivation of the secant stiffness matrix is more complex in this case. Further details and other examples of application can be found in [50].

11. ACKNOWLEDGEMENTS

William T. Matias gratefully acknowledges the finnancial support received from the CAPES programme of Brasil.

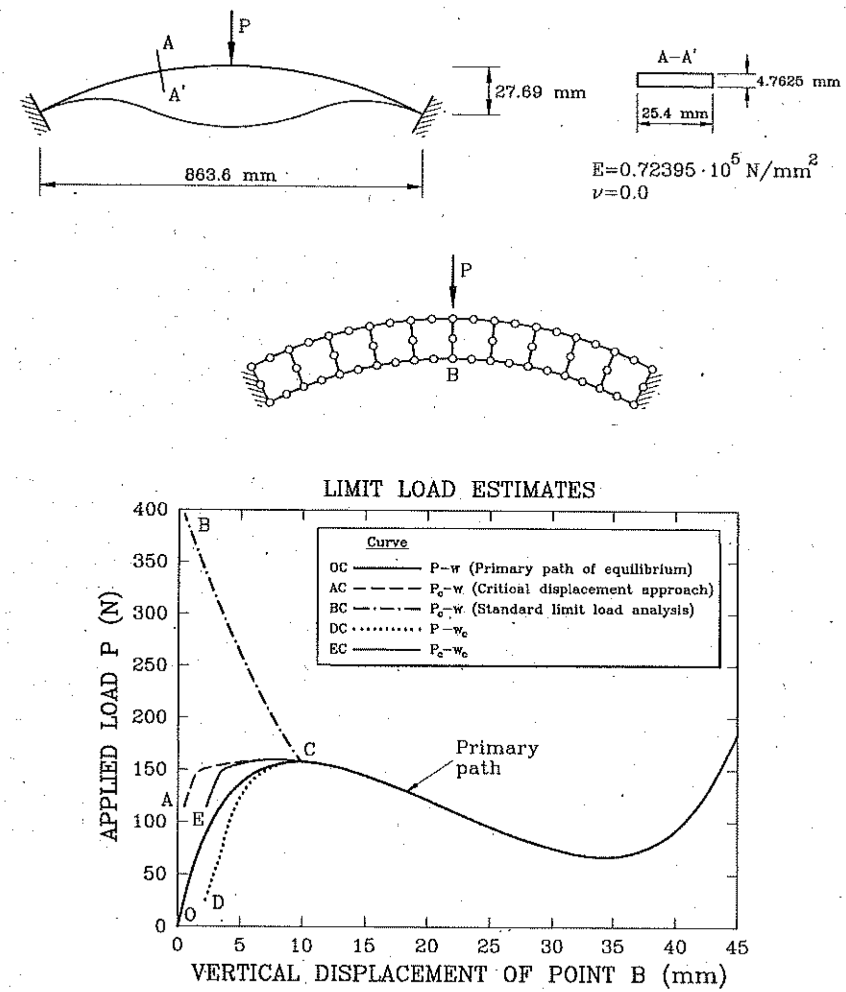

Figure 8. Clamped shallow arch. Load-displacement curve and limit load estimates

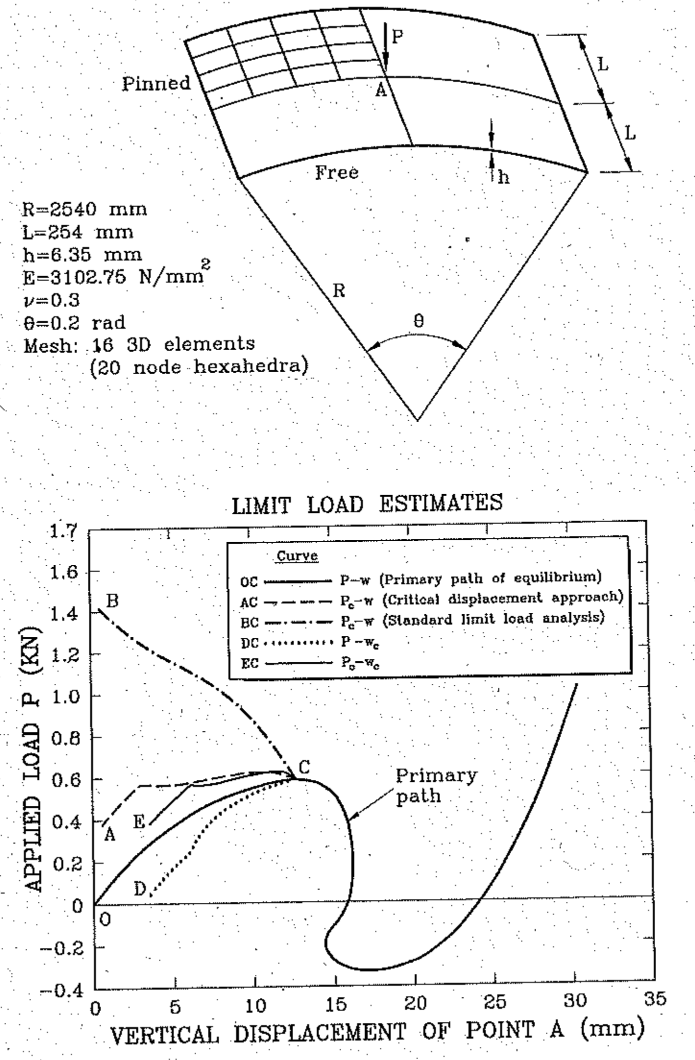

Figure 9. Cylindrical shell. Load-displacement curve and limit load estimates

12. REFERENCES

[1] J. Weinitschke, "On the calculation of limit and bifurcation points in stability problems of elastic shells", *Int. J. Solids Structures*, Vol. **21**, 1, 1985.

[2] R. Seydel, "Numerical computation of branch points in nonlinear structural analysis", *Numer. Math.*, Vol. 33, 339–352, 1979.

[3] P. Wriggers, W. Wagner and C. Miehe, "A quadratically convergent procedure for the calculation of stability points in finite element analysis", *Comp. Methods in App. Mech. and Engrg*, **70**, 329–347, 1988.

[4] P. Wriggers and J.C. Simo, "A general procedure for the direct computation of turning and bifurcation points", *Int. J. for Numerical Methods in Engrg.*, Vol. **30**, 155–176, 1990.

[5] G. Skeie and C.A. Felippa., "Detecting and traversing bifurcation points in nonlinear structural analysis", *Int. J. of Space Structures*, Vol. **6**, 2, 77–98, 1991.

[6] W. Wagner, "Calculation of bifurcation points via fold curves", *Nonlinear Computational Mechanics*, State–of–the–Art, eds. Wriggers P. and Wagner W., 70–84, 1991.

[7] Z. Waszczysztn, "Numerical problems of nonlinear stability analysis of elastic structures", *Computers and Structures*, Vol. **17**, 1, 13–24, 1983.

[8] E. Riks, "Bifurcation and stability, a numerical approach", *Proceedings of the International Conference on Innovative Methods for Nonlinear Problems*, eds. Liu W.K., Belytschko T. and Park K.C., Pineridge Press International Limited, 313–344, 1984.

[9] M.A. Fujikake, "Simple approach to bifurcation and limit point calculations", *Int. J. for Numer. Meth. in Engrg.*, Vol. **21**, 183–191, 1985.

[10] F. Nishino, W. Hartono, O. Fujiwara and P. Karasudhi, "On tracing bifurcation equilibrium paths of geometrically nonlinear structures", *Structural Engrg./Earthquake Engrg.*, Vol. **4**, 1, Proc. of JSCE 380/I–7, April, 11s–17s, 1987.

[11] W. Wagner and P. Wriggers, "A simple method for the calculation of postcritical branches", *Eng. Comput.*, Vol. **5**, June, 103–109, 1988.

[12] R. Kouhi and M. Mikkola, "Tracing the equilibrium path beyond simple critical points", *Int. J. for Numer. Methods in Engrg.*, Vol. **28**, 2922–2941, 1989.

[13] E. Stein, W. Wagner and P. Wriggers, "Nonlinear stability analysis of shell and contact–problems including branch–switching", *Computational Mechanics*, Vol. **5**, 428–446, 1990.

[14] H.A. Mang, "On bounding properties of eigenvalues from linear initial FFC stability analysis of thin elastic shells with respect to stability limits from geometrically non linear prebuckling analysis", *Int. J. Num. Meth. Engrg.*, 1991.

[15] P. Fuji, B.C. Perez and K.K. Choong, "Selection of the control parameters in displacement incrementation", *Comp. and Struc.*, Vol. **42**, 2, 167–174, 1992.

[16] E. Riks, "An incremental approach to the solution of snapping and buckling problems", *Int. J. Solids Structures*, Vol. **15**, 529–551, 1979.

[17] E. Riks, "Some computational aspects of the stability analysis of nonlinear structures", *Computer Methods in Applied Mechanics and Engineering*, Vol.

47, 219–259, 1984.

[18] K.K. Choong and Y. Hangai, "Review on methods of bifurcation analysis for geometrically non linear structures", Bolletin of IASS, Vol. **34**, 112, pp. 133–149, 1993.

[19] E. Oñate, J. Oliver, J. Miquel and B. Suárez, "A finite element formulation for geometrically non linear problems using a secant matrix", in *Proceedings of international conference on Computational Mechanics, May 25–29, Tokyo*, S. Atluri and G. Yagawa (eds.), Springer-Verlag, 1986.

[20] E. Oñate, "Possibilities of the secant stiffness matrix for non linear finite element analysis", in *Non Linear Engineering Computations*, N. Bicanic et al. (eds.), Pineridge Press, 1991.

[21] E. Oñate, "On the derivation and possibilities of the secant stiffness matrix for non linear finite element analysis", *Computational Mechanics*, (1995).

[22] E. Oñate and W. Matias, "A critical displacement approach for prediction structural instability". Submitted to *Comp. Meth. Appl. Mech. Engng.*, May 1995.

[23] H. Duddeck, B. Kroplin, D. Dinkler, J. Hillmann, W. Wagenhuber, "Non linear computations in Civil Engineering Structures " (in German), DFG Colloquium, 2–3 March 1989, Springer–Verlag, Berlin, 1989.

[24] B. Kroplin, M. Wilhelm and M. Herrmann, "Unstable phenomena in sheet metal forming processes and their simulation", VDI. Berichte NR. 894, 137–52, 1991.

[25] B. Kroplin, "Instability prediction by energy perturbation" in *Numerical Methods in Applied Sciences and Engineering*, H. Alder, J. C. Heinrich, S. Lavanchy, E. Oñate and B. Suarez (eds.), CIMNE, Barcelona, 1992.

[26] J.M.T. Thompson and G.W. Hunt, "A general theory of elastic stability", John Wiley and Sons, 1973.

[27] M. Pignataro, N. Rizzi and A. Luongo, "*Stability, Bifurcation and Postcritical Elastic Structures*", Elsevier, 1991.

[28] B. Kroplin, D. Dinkler and J. Hillmann, "An energy perturbation method applied to non linear structural analysis", *Comp. Meth. Appl. Mech. Engng.* , **52**, 885–97, 1985.

[29] B. Kroplin and D. Dinkler, "A material law for coupled local yielding and geometric inestability", *Engineering Computions* Vol. **5**, 3, pp. 210–216, 1988.

[30] B. Kroplin and D. Dinkler, "Some thoughts on consistent tangent operators in plasticity" in *Computational Plasticity* D.R.J. Owen, E. Hinton and E. Oñate (eds.), Pineridge Press/CIMNE, 1990.

[31] E. Carrera, "Sull' uso dell' operatore secante in analisi non lineare di strutture multistrato con il metodo degli elementi finiti", XI Congressò Nazionale AIMETA, Trento, 28 September–2 October, 1992.

[32] E. Carrera, "On the application of the energy perturbation method to higher non linear–problems", VIII Convegno Italiano di Meccanica Computazionale, AIMETA, Politecnico di Torino, 15–17 January, pp. 149–254, 1994.

[33] R.H. Mallet and P.V. Marcal, "Finite element analysis of non–linear structures", *J. Struct. Div.*, ASCE, **14**, pp. 2081–2105, 1968.

[34] S. Rajasekaran and D. W. Murray, "Incremental finite element matrices",*J. Struct. Div.* , ASCE, **99**, pp. 2423–2438, 1973.

[35] C. Felippa, "Discussions on reference [34] ", *J. Struct. Div.* , ASCE, **100**, pp. 2519–2521, 1974.

[36] C. Felippa and L.A. Crivelli, "The core–congruential formulation of geometrically non–linear TL finite elements", in *Non–Linear Computational Mechanics. The State – of – the – Art.*, P. Wriggers and W. Wagner (eds.), Springer–Verlag, Berlin, 1991.

[37] C. Felippa, L.A. Crivelli and B. Haugen, "A survey of the core–congruential formulation for geometrically non–linear TL finite elements", *Archives of Comp. Meth. in Engrg.*, Vol. **1**, 1, 1–48, 1994.

[38] R.D. Wood and B. Schrefler, "Geometrically non–linear analysis –A correlation of finite element notations" *Int. J. Num. Meth. Engng.*, **12**, 635–42, 1978.

[39] M. Badawi and A.R. Cusens, "Symmetry of the stiffness matrices for geometrically non linear analysis", *Communications in Appl. Num. Meth.*, **8**, 135–40, 1992.

[40] K.J. Bathe, "*Finite element procedures in engineering analysis*", Prentice Hall, 1982.

[41] O.C. Zienkiewicz and R.L. Taylor, "*The finite element method*", McGraw-Hill, Vol. I (1989) and Vol. II (1991).

[42] G.H. Powell and J. Simons, "Improved iteration stretegy for non–linear structures", *Int. J. Num. Meth. Engng.*, **17**, 1455–1467, 1981.

[43] M. Papadrakakis, "Post–buckling analysis of spatial structures by vector iteration methods", *Computers and Structures*, **14**, 5-6, 393–402, 1981.

[44] R. Irles, "Un modelo numérico para el análisis del colapso en entramados metálicos", Ph. D. Tesis (in Spanish), Universidad Politécnica de Valencia, 1985.

[45] H.H. Kwok, M.P. Kamat and L.T. Watson, "Location of stable and unstable equilibrium configurations using a model truss region quasi–Newton method and tunnelling", *Computers and Structures*, **21**, 909–916, 1985.

[46] K. Kondoh and S.N. Atluri, "Influence of local buckling on global instability: simplified, large deformation, post–buckling analysis of plane trusses", *Computers and Structures*, **21**, 4, 613–627, 1985.

[47] D.J. Dawe, "Finite deflection analysis of shallow arches by discrete element method", *Int. J. Num. Meth. Engng.*, **3** (4), 1971.

[48] J. Oliver and E. Oñate, "A total Lagrangian formulation for the geometrically non linear analysis of structures using finite elements. Part II. Arches, frames and axisymmetric shells", *Int. J. Num. Meth. Engng.*, **23**, 253–274, 1986.

[49] J.C. Simo, D.D. Fox and M.S. Rifai, "Formulation and computational aspects of a stress resultant geometrically exact shell model", published on *Computational Mechanics of Nonlinear Response of Shells*, W.B. Krätzig and E. Oñate (Eds.), Springer-Verlag, 1990.

[50] W.T. Matias, "Finite element structural instability analysis using a critical displacement method", Ph.D. Thesis (in Spanish), Univ. Politècnica de Catalunya, Barcelona, Spain, 1996